CHINESE GEOGRAPHICAL SCIENCE
Volume 15, Number 3, pp.231–237, 2005
Science Press, Beijing, China

IMAGE ANALYSIS OF GEOSTATIONARY METEOROLOGICAL SATELLITE FOR MONITORING MOVEMENT OF MESOSCALE CONVECTIVE SYSTEMS OVER TIBETAN PLATEAU

GUO Zhong-yang[1], DAI Xiao-yan[1], WU Jian-ping[1], LIN Hui[2]
(*1. Ministry of Education Key Laboratory of Geographic Information Science, East China Normal University, Shanghai 200062, P. R. China; 2. Department of Geography and Resource Management & Joint Laboratory for GeoInformation Science, The Chinese University of Hong Kong, Hong Kong, P. R. China*)

ABSTRACT: Disaster weather forecasting is becoming increasingly important. In this paper, the trajectories of Mesoscale Convective Systems (MCSs) were automatically tracked over the Chinese Tibetan Plateau using Geostationary Meteorological Satellite (GMS) brightness temperature (Tbb) from June to August 1998, and the MCSs are classified according to their movement direction. Based on these, spatial data mining methods are used to study the relationships between MCSs trajectories and their environmental physical field values. Results indicate that at 400hPa level, the trajectories of MCSs moving across the 105°E boundary are less influenced by water vapor flux divergence, vertical wind velocity, relative humidity and *K* index. In addition, if the gravity central longitude locations of MCSs are between 104°E and 105°E, then geopotential height and wind divergence are two main factors in movement causation. On the other hand, at 500hPa level, the trajectories of MCSs in a north-east direction are mainly influenced by *K* index and water vapor flux divergence when their central locations are less than 104°E. However, the MCSs moving in an east and south-east direction are influenced by a few correlation factors at this level.

KEY WORDS: Tibetan Plateau; Mesoscale Convective Systems; automatically tracking; spatial data mining

CLC number: P407 Document code: A Article code: 1002-0063(2005)03-0231-07

1 INTRODUCTION

Recent evidence has indicated that disaster weather conditions, such as storms, typhoons, and intensive convection, are directly influenced by Mesoscale Convective Systems (MCSs) (JIANG and FAN, 2002). Also, the MCSs, which move out of the Tibetan Plateau, are related to intensive precipitation in the Changjiang (Yangtze) River Basin and the southwestern region of China (SHAN *et al*., 2003). To date, however, development theories of MCSs and their structure are not yet clear, due to restrictions on time and space scales in traditional observation data. Therefore, it is difficult to predict the activity of MCSs, especially in the Chinese Tibetan Plateau (Fig.1).

However, with the development of meteorological satellite remote sensing technology, it has been possible to collect increasing amounts of image data to be stored in different databases. As a result, substantial information related to disaster weather has been hidden in these data. In most cases, the image data files are too large to be extracted in a reasonable amount of time using traditional data analysis methods, including numerical models. Thus spatial data mining methods are emerging to extract implicit knowledge, data relations, or other patterns not explicitly stored in databases (KOPERSKI and HAN, 1995).

Among existing disaster weather forecasting applications using spatial data mining, the ATOMOSPHER system (LEE and LIU, 1999, 2000) is a successful example. In this system, 120 TC (Tropical Cyclone) cases appearing in the period from 1985 to 1998 were used to test the effectiveness of the methods used in the ATOMOSPHER system. The system achieved a 97% accuracy

Received date: 2005-06-18
Foundation item: Under the auspices of the National Natural Science Foundation of China (No. 40371080), Key Foundation Supported by Ministry of Education (No. 104083), Foundation of Wuhan University State Key Laboratory of Information Engineering in surveying, mapping and remote sensing (No. WKL (03) 0103)
Biography: GUO Zhong-yang (1965–), male, a native of Shengxian of Zhejiang Province, professor, specialized in spatial data mining. E-mail: zyguo@geo.ecnu.edu.cn

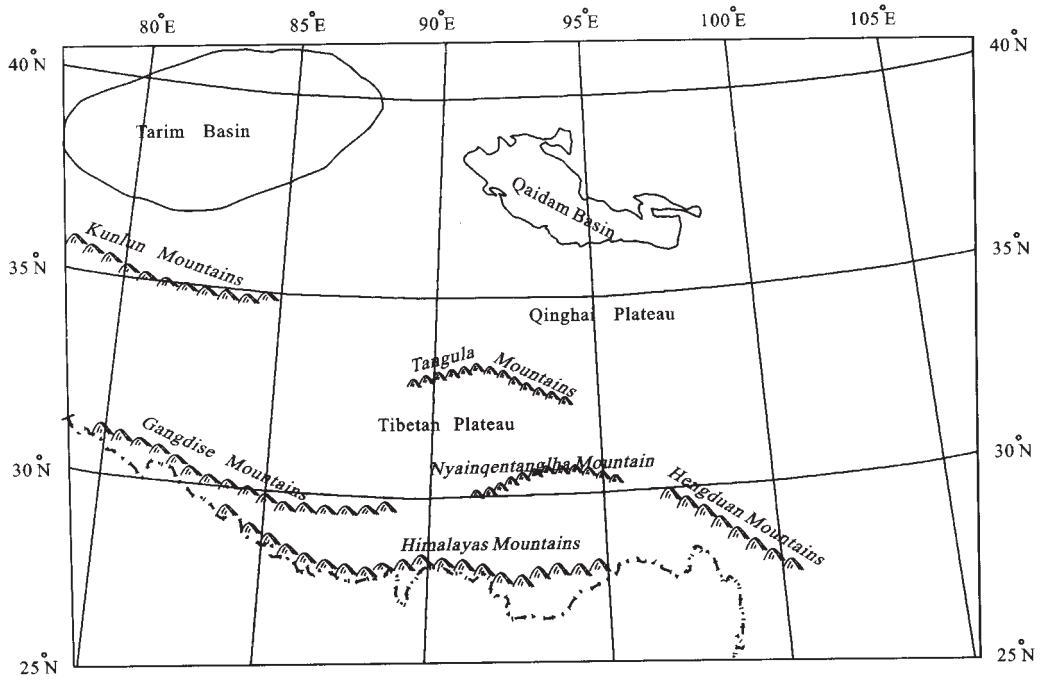

Fig.1 The Tibetan Plateau region

rate for correct classification and an 86% correct prediction rate in TC tracking. In another application, KITAMOTO (2002) used 34 000 typhoon images as a testbed to discover the statistical properties of typhoon cloud patterns. KITAMOTO then used a similarity-based approach to predict typhoons based on past typhoon cloud patterns and existing cloud patterns. In another project, ZHOU *et al*. (1999) used related images to develop new neural network models and increase knowledge about typhoons.

In this paper, spatial data mining methods are used to analyse the relationships between MCSs trajectories and their environmental physical field values through meteorological satellite remote sensing imaging in the Tibetan Plateau from June to August 1998. The paper will begin with describing spatial data mining methods, data sources and MCSs tracking techniques. This will be followed by an analysis of MCSs shape classification. Trajectories of MCSs, feature values abstraction and results will then be discussed, with subsequent conclusions and recommendations.

2 DATA SOURCES

GMS brightness temperature (Tbb) and high resolution limited area analysis and forecasting system (HLAFS) values provided by China National Satellite Meteorological Center from June to August 1998 are used in this study. For data range of Tbb, latitude is from 0° to 50°N and longitude is from 80° to 150°E. HLAFS, latitude is from 15° to 64°N and longitude is from 70° to 145°E. On the other hand, Tbb is 0.5° latd. × 0.5° long. resolution, i.e., each pixel of an image represents a 0.5° × 0.5° latitude and longitude. HLAFS is 1° latd. × 1° long. resolution. Due to the great error of GMS brightness temperature (Tbb) data to the west of 80° E over the Tibetan Plateau, consequently, in this project, study area that is from 27° to 40° N and 80° to 105° E, is selected. Meanwhile, the elevation of the Tibetan Plateau is 4000–5000m, and the levels of 400hPa and 500hPa represent air conditions of nearly ground and lower layers at the Plateau, respectively. Consequently, 400hPa and 500hPa are included in this study. Based on these, HLAFS datasets, including geopotential height, temperature, vorticity, wind divergence, water vapor flux divergence, vertical wind velocity, pseudo-equivalent potential temperature, K index and relative humidity in different UTC (Universal Time Coordinate) (00:00 UTC, 12:00 UTC, 24:00 UTC) are used to determine the relationships between MCSs trajectories and environmental physical field values. For example, the distribution of pseudo-equivalent potential temperature with height and K index can reveal the stability of air layer convective activity. Furthermore, according to the definition of MCSs (MADDOX, 1980), the study focuses on MCSs that cover at least 3 connected pixels having Tbb ≤ 241K in each Tbb image, and lasting for at least 3 consecutive hours.

3 METHODS

3.1 MCS Tracking

Numerous studies have devised methods to automatically track convective systems using meteorological satellite remote sensing image data (ARNAUD *et al*., 1992; MACHADO *et al*., 1998; CARVALHO and JONES, 2001). For example, CARVALHO and JONES (2001) developed an efficient method based on maximum spatial correlation tracking technique (MASCOTTE), to monitor the evolution of convective systems (CS), using satellite images. The results indicated that MASCOTTE is a valuable approach to understanding the variability of CS. ARNAUD *et al*. (1992) established an automatic method to track and characterize (CS) on Meteosat infrared images according to the variability of area in consecutive hours.

In this paper, using the methods developed by ARNAUD *et al*. (1992), the trajectory of each MCS is tracked as follows:

(1) To detect whether MCS, C, in hour h_i is the same as C' in the next available image in hour h_{i+1}, the ratio $A'c/Ac$ is computed, where Ac is the area of MCS (C) in hour h_i, and $A'c$ is the overlapping area of MCS (C') in hour h_{i+1} with C in hour h_i. If its value is at least 0.5, then C and C' are regarded as the same MCS.

(2) If two MCSs, C_i and C_j, in hour h_1 are merged to C' in the next hour h_2, one is regarded as being "still alive while another disappeared" in h_2. The selection is based on the area: if the area of C_i is larger than that of C_j, then C' is the continuation of C_i, otherwise C' is the continuation of C_j.

(3) When an MCS, C, is split into two or more smaller MCSs, $C'_1, C'_2, \ldots, C'_n$ in the next hour, and the overlapping area of C with some of the small MCSs is greater than the overlapping threshold, then, C'_i, the largest, is chosen as the same MCS as C and the others are regarded as new MCSs.

3.2 Shape Identification of MCS

The shape of MCSs is also an important factor influencing their movement. Therefore, before spatial data mining, it is necessary to identify the shape of MCSs. The identification procedure can be divided into two steps. In step one, the gravity centre coordinates of MCSs are calculated according to the following formula:

$$x_0=\frac{\sum_{i=1}^{n} x_i t_i}{\sum_{i=1}^{n} t_i}, \quad y_0=\frac{\sum_{i=1}^{n} y_i t_i}{\sum_{i=1}^{n} t_i} \tag{1}$$

where x_0 and y_0 are the gravity centre coordinates of MCSs, x_i, y_i, and t_i represent the longitude, latitude and brightness temperature (Tbb) of the MCSs pixels, respectively, while n represents the number of pixels included by the MCSs. Secondly, the MCSs shape will be determined by ellipse equation using the least squares method, and based on these, the long axis length and short axis length of the ellipse will be obtained. Consequently, the shape of MCSs can be defined according to the ratio of the short axis length to the long axis length, i.e., the shape of MCSs is defined as circular (C) when the ratio is in [0.9, 1.0] and ellipse (E) when the ratio is in [0.7, 0.9). Otherwise, the shape of MCSs is defined as others (O).

3.3 Classification of MCS

Based on previous tracking methods, MCSs are classified into 4 types according to their trajectories over the Tibetan Plateau, i.e., if MCSs move across the 105°E boundary, then they are considered to have moved out of the Tibetan Plateau, and their movement direction is defined E, NE and SE, respectively. Otherwise, it is defined 'stay-in'. Table 1 shows the classification results.

Table 1 Number of MCSs in different directions over Tibetan Plateau from June to August 1998

Month	Number of MCSs in different directions			
	Stay-in	E	SE	NE
June	209	9	3	3
July	246	11	–	4
August	239	21	2	2
Total	694	41	5	9

From Table 1, it can be seen that 7.34% of the total number of MCSs move across the 105°E boundary, while 74.5%, 9.1% and 16.4% of the MCSs moving across the boundary move to E, SE and NE, respectively.

3.4 Trajectories of MCS

Fig. 2a–c shows the trajectories of MCSs moving out of the Tibetan Plateau from June to August 1998. From Fig. 2a, it can be seen that the initiation locations of most of the MCSs moving to the southeast and northeast are less than 100°E, and the lengths of MCSs trajectories are relatively long. On the other hand, the initiation locations of most of the MCSs moving to the east are between 100°E and 105°E, with one exception. Among these MCSs, the lengths of trajectories are relatively short. Moreover, in this month, the initiation locations of most of the MCSs are less than 36°N along latitude orientation.

The trajectories of MCSs moving across the Tibetan

Plateau in July are presented in Fig. 2b, which demonstrates that there are no MCSs moving to the southeast during this month, while the initiation locations of most of the MCSs are between 100°E and 105°E. Furthermore, with one exception, the lengths of MCSs trajectories are relatively short during this month.

Fig. 2c shows that the features of MCSs trajectories in August are similar to those of July, the difference between MCSs trajectories in August and in July being that the initiation locations are less than 36°N along latitude orientation in July, while the initiation locations distribution of MCSs in August are more homogeneous along latitude orientation.

On the other hand, Fig. 2a–c also shows that the initiation locations of most of MCSs from June to August 1998 are between 95°E and 105°E. Therefore, in the course of spatial data mining, the initiation gravity center location of each MCS is defined near 100°E.

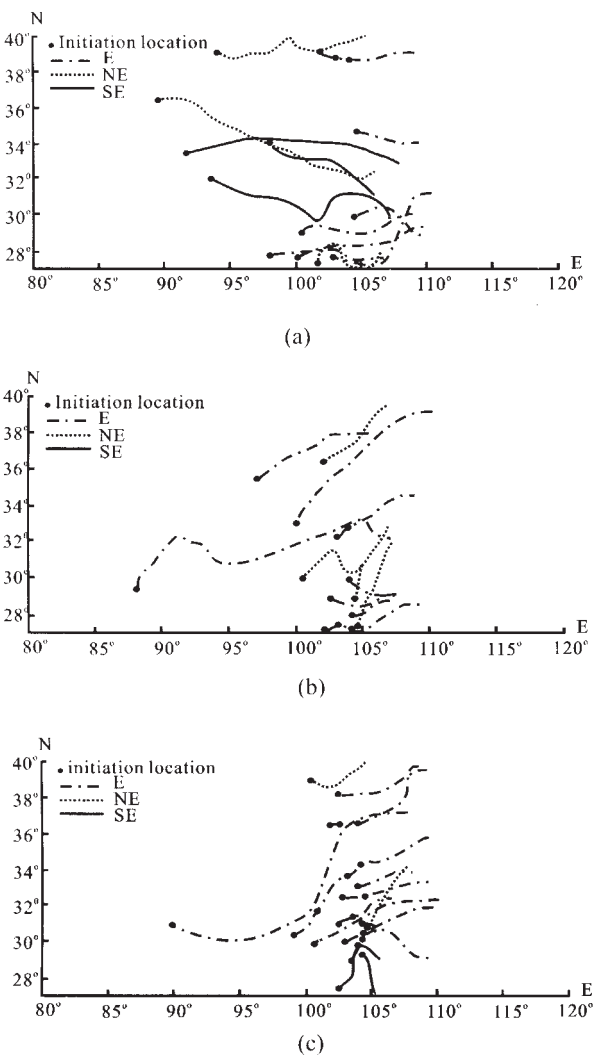

Fig. 2 Trajectories of MCSs moving out of the Tibetan Plateau from June to August 1998

3.5 Feature Values Abstraction

Weather forecasting is critical to people's daily life and to sustainable development. To make up for the shortage of ground observation stations, high spatio-temporal resolution meteorological satellites have provided a meaningful data source. Consequently, finding the optimal method for extracting useful information from the observation data has become increasingly important.

Fig. 3a–d shows examples of the relationships between the trajectories of MCSs moving out of the Tibetan Plateau, and vorticity values around its center at 00UTC in 400hPa level on 7 June, 30 June, 9 July and 11 August. Using the figure, the relationships between the trajectories of MCSs and vorticity values cannot be clearly understood. However, according to the results of previous tracking, the MCSs shown in Fig. 3a–d move out of the Plateau in an easterly direction. Clearly, therefore, some relationships must exist between them. This is important, therefore, in abstracting useful information on what influences the trajectories of MCSs, from wide environmental physical field values. In the following section, the processing approach used for the given data according to the results of MCSs tracking will be described.

First, in the course of extracting information on factors influencing the trajectories of MCSs, the parameters, including geopotential height (H), temperature (T), relative humidity (RH), vorticity (VOR), wind divergence (DIV), vertical wind velocity (W), water vapor flux divergence ($IFVQ$), pseudo-equivalent potential temperature (θSE), K index, area of MCSs, the average lowest temperature (Tbb), location (longitude and latitude) and the shape of MCSs are used in this study. Second, an MCS is centred at (x_1, y_1) when it moves to near 100°E at the time UTC=H_m. Choose the HLAFS at UTC=H_h (either equals to 00, 12 or 24UTC) where H_h is the nearest 00/12/24 UTC to H_m. If the MCS is centred at (x_2, y_2) at the time UTC=H_m+2, then three areas (A, B, C), which are near the MCSs at the time UTC=H_m+2, will be defined according to the direction in which the MCSs are moving. Each area (A, B, C) is 1° latd. × 3° long. For each of the 9 HLAFS attributes, the average for A, B and C will be found respectively, then D_{b-a} and D_{b-c} are defined as the difference in the average in areas B and A and that of areas B and C respectively (Fig. 4).

Based on the information above, a vector consisting of the following fields for each MCS is formed:

– D_{b-a} for each of the 9 HLAFS attributes (H, T, DIV, VOR, θSE, K, $IFVQ$, W, RH)

– D_{b-c} for each of the 9 HLAFS attributes

– Area of MCSs when UTC=H_m

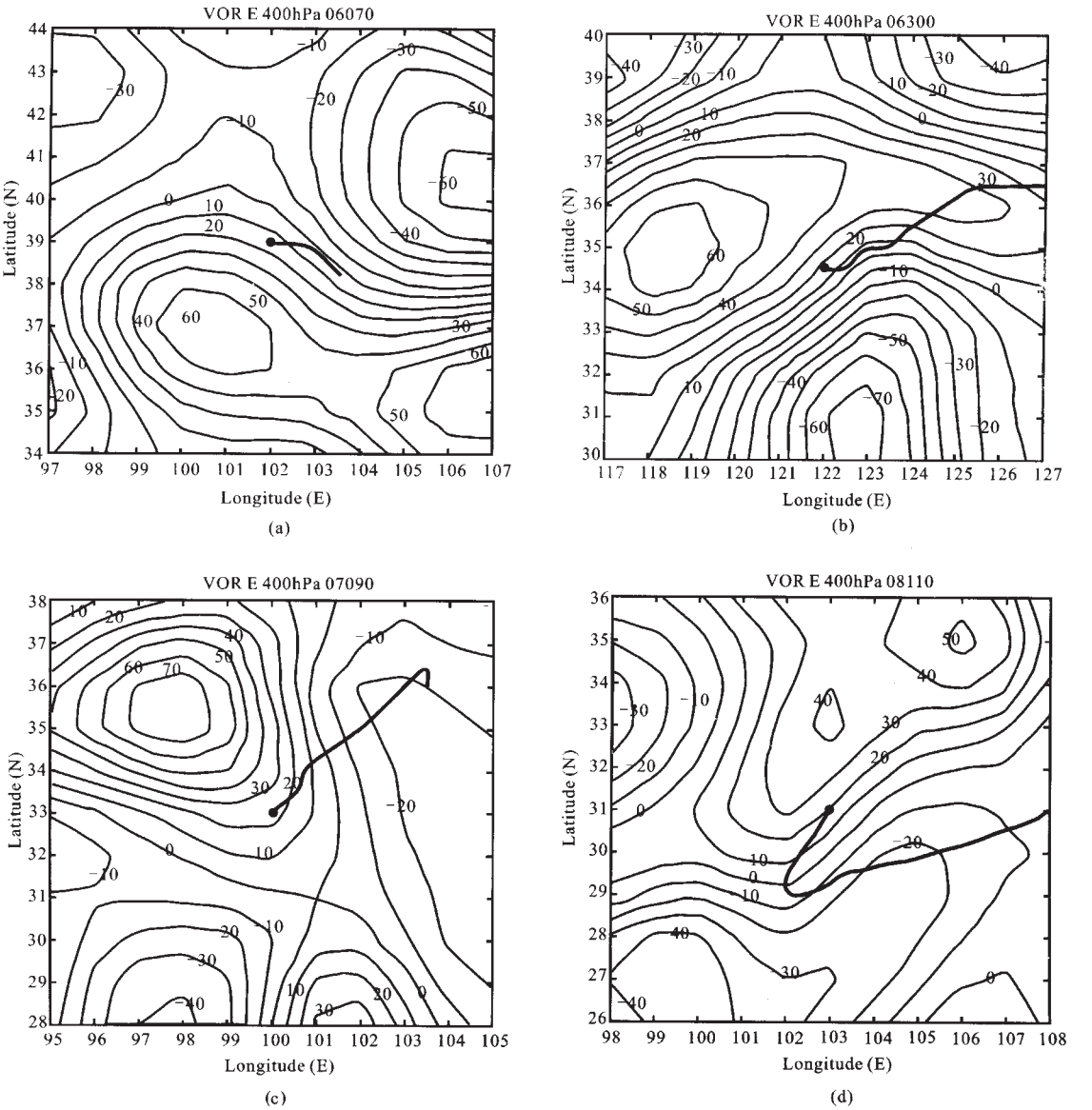

Fig.3 Chart of the relationships between the trajectories of MCSs and vorticity values ($\times 10^{-6}$/s)

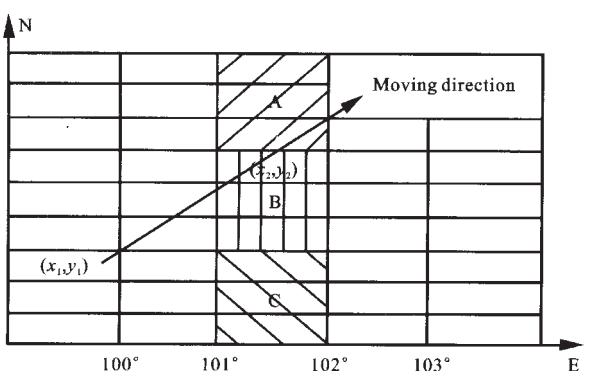

Fig.4 Relevant area of spatial data mining

– Shape of MCSs when UTC = H_m

– Position of MCSs when UTC = H_m

– Average lowest Tbb value of MCSs when UTC = H_m

4 RESULTS AND DISCUSSION

In spatial data mining, the decision tree is the main technique used to classify huge amounts of data. The data classification procedure can always be separated into two steps, i.e., growing and pruning (BREIMAN *et al*., 1984). There are different approaches to classify object data according to data size stored in databases. For example, earlier algorithms for decision tree induction, ID3 and CART (WEISS and KAPOULEAS, 1989; HOLDER, 1995), have high classification accuracy and efficiency when data size is small. However, they are not suited to classification of large data sizes. Consequently,

in this paper, C4.5 (SALVATORE, 2002) is taken to mine hidden knowledge of influencing MCSs movement. It is an algorithm for inducing classification rules in the form of decision trees from a set of given data. It constructs the decision tree with a "divide and conquer" strategy. After each tree is generated, it is pruned in an attempt to simplify it. The advantages of this method are that not only can it mine useful information and knowledge from large databases, but it also has high accuracy and efficiency.

Table 2 and Table 3 show the classification rules, which have been pruned, of influencing MCSs moving out of the Tibetan Plateau in 400hPa and 500hPa level, where the symbols and units of different parameters are defined as follows: geopotential height (H)→10^{-1}gpm, temperature (T)→℃, relative humidity (RH)→%, vorticity (VOR)→10^{-6}/s, wind divergence (DIV)→10^{-6}/s, vertical wind velocity (ω)→10^{-5}hPa/s, water vapor flux divergence ($IFVQ$)→10^{-10}g/(cm^2·hPa·s), pseudo-equivalent potential temperature (θSE)→℃, K index, area→km^2, the average lowest temperature (tbb)→℃, position (longitude and latitude) and shape. The form of rules is "$P_1\wedge\cdots\wedge P_m\rightarrow Q_1\wedge\cdots\wedge Q_n$", where P_1,…,P_m, Q_1,…,Q_n are attribute data. The rules are interpreted as when the pattern "$P_1\wedge\cdots\wedge P_m$" develops, the pattern "$Q_1\wedge\cdots\wedge Q_n$" also develops with a certain probability. In table 2, the meaning of H_{bc} is the difference of geopotential height in area B and area C. E (16/3.7) means that the number of MCSs which satisfy the rule is 16, but 3.7 MCSs remain in the Tibetan Plateau, i.e., the accuracy is 76.9% when this rule is applied to determine the movement of MCSs across 105°E, and the meaning of others is similar. Consequently, from Table 2, it can be found that the geopotential height in the south of MCSs center is higher than in the north in 400hPa level. If the initiation gravity center location of MCSs is greater than 104°E and $H_{bc}\leqslant -1$, then wind divergence is a main factor in influencing the movement of MCSs. The physical meaning of the rules can be explained in the following example: according to rule 1, it represents that, when MCSs exist between 104°E and 105°E and the geopotential height in the south of MCSs centre is higher than that in the north and wind divergence in the south of MCSs centre is lower than that in the north, the MCSs exist in an air convergence area. According to the rule of influencing MCSs movement, the two environmental physical field values reveal that they will influence MCSs movement out of the Plateau. Other rules can be explained in the same manner. By and large, at this level, the MCSs moving out of the Tibetan Plateau are mainly related to the differences of geopotential height, vorticity, wind divergence along latitude orientation, area, and longitude location of MCSs centre. On the other hand, the results also show that the trajectories of MCSs moving out of the Plateau are not related to the differences in relative humidity, vertical wind velocity, water vapor flux divergence, K index along latitude orientation, as well as the average lowest temperature and latitude location of MCSs centre. Therefore, the features of the environmental physical field values in 400hPa level can be summarized as follows:

(1) The movement of MCSs across the 105°E boundary is less influenced by water vapor flux divergence, vertical wind velocity, relative humidity and K index.

Table 2 Classification rules influencing MCSs trajectories in 400hPa level

Index	Rule
1	$H_{bc}\leqslant -1\wedge 104°\text{E}<\text{Longitude}<105°\text{E}\wedge DIV_{bc}\leqslant 6\rightarrow$ E (16/3.7)
2	$H_{bc}\leqslant -1\wedge 102°\text{E}<\text{Longitude}\leqslant 104°\text{E}\wedge\text{Area}>41250\,T_{ba}>-1\wedge VOR_{bc}>-28\rightarrow$ E (12/2.5)
3	$H_{bc}\leqslant -1\wedge\text{Longitude}\leqslant 102°\text{E}\wedge\text{Area}>233750\wedge\text{Shape is others}\wedge VOR_{bc}\leqslant 22\rightarrow$ E (7/2.4)
4	$H_{bc}\leqslant -1\wedge\text{Longitude}\leqslant 102°\text{E}\wedge\text{Area}>233750\wedge\theta SE_{bc}>-3\wedge\theta SE_{ba}\leqslant 2\wedge\text{Shape is circle}\rightarrow$E (3/2.1)
5	$H_{bc}\leqslant -1\wedge\text{Longitude}\leqslant 102°\text{E}\wedge\text{Area}>233750\wedge\theta SE_{bc}\leqslant -3\rightarrow$NE (3/2.1)

Table 3 Classification rules influencing MCSs trajectories in 500hPa level

Index	Rule
1	$101.5°\text{E}<\text{Longitude}\leqslant 104°\text{E}\wedge\text{Area}\leqslant 233750\wedge IFVQ_{bc}\leqslant -74\rightarrow$NE (2/1)
2	$101.5°\text{E}<\text{Longitude}\leqslant 104°\text{E}\wedge\text{Area}\leqslant 233750\wedge H_{ba}\leqslant 17\wedge K_{ba}\leqslant 12\wedge T_{ba}>9\wedge IFVQ_{bc}>-74\wedge DIV_{bc}\leqslant 6\rightarrow$ E (10)
3	$101.5°\text{E}<\text{Longitude}\leqslant 104°\text{E}\wedge\text{Area}\leqslant 233750\wedge H_{ba}>17\wedge K_{ba}\leqslant 12\wedge T_{ba}>9\wedge IFVQ_{bc}>-74\wedge IFVQ_{ba}>2\wedge DIV_{bc}\leqslant 6\rightarrow$ E (3)
4	$\text{Longitude}\leqslant 104°\text{E}\wedge\text{Area}>233750\wedge K_{bc}\leqslant 0\rightarrow$NE (3/1)
5	$\text{Longitude}\leqslant 104°\text{E}\wedge\text{Area}>233750\wedge H_{ba}\leqslant 9\wedge\theta SE_{bc}\leqslant 0\rightarrow$SE (2/1)
6	$\text{Longitude}\leqslant 104°\text{E}\wedge\text{Area}>233750\wedge\omega_{ba}\leqslant 138\wedge H_{ba}>9\wedge K_{bc}>0\wedge\theta SE_{bc}\leqslant 0\rightarrow$E (8)
7	$\text{Longitude}\leqslant 104°\text{E}\wedge\text{Area}>233750\wedge\omega_{ba}>138\wedge H_{ba}>9\wedge K_{bc}>0\wedge\theta SE_{bc}\leqslant 0\rightarrow$SE (3/1)
8	$\text{Longitude}\leqslant 104°\text{E}\wedge\text{Area}>521250\wedge\theta SE_{bc}>0\wedge DIV_{ba}>-10\rightarrow$E (2)
9	$104°\text{E}<\text{Longitude}<105°\text{E}\wedge\text{Area}>26250\rightarrow$E (14)
10	$104°\text{E}<\text{Longitude}<105°\text{E}\wedge\text{Latitude}>30.5\wedge\text{Area}\leqslant 26250\rightarrow$E (2)

(2) The difference of geopotential height around gravity center location of MCSs is a main factor in determining their movement, i.e., the movement of MCSs is mainly influenced by air flow.

(3) If gravity central longitude locations of MCSs are between 104°E and 105°E, then geopotential height and wind divergence are two main factors in causing their movement.

On the other hand, from Table 3, the features influencing MCSs movement in 500hPa level can be summarized as follows:

(1) In this level, the trajectories of MCSs moving out of the Tibetan Plateau are less influenced by vorticity, relative humidity and shape.

(2) If gravity central longitude locations of MCSs are less than 104°E, the trajectories of MCSs, when moving north-easterly, are mainly related with area, K index and water vapor flux divergence.

(3) If gravity central longitude location of MCSs is between 104°E and 105°E, while its area is greater than 26 250km^2, then the MCSs must move out of the Tibetan Plateau.

From the analysis set out above, it can be found that the rules obtained in 400hPa and 500hPa are different, the also reason being that environmental physical field values are different in 400hPa and 500hPa. Results indicate that it is feasible to predict the trajectories of MCSs based on their environmental physical field values at the Tibetan Plateau. Furthermore, it is also important to discuss the relationships between the movement of MCSs and intensive precipitation forecasting in the Yangtze River Basin and in the south-west region of China.

5 CONCLUSIONS

Various rules influencing MCSs movement at the Tibetan Plateau in China have been revealed that using spatial data mining techniques, and the development of favorable environmental physical field rules of influencing MCSs movement across Tibetan Plateau produces important results. These rules can be used to reveal the relationships between the MCSs trajectories at the plateau and intensive precipitation forecasting in the Changjiang River Basin and in the southwestern region of China. Consequently, this information is of great value in limiting the damage caused by disaster weather. The mathematical model of MCSs trajectories and their environmental physical field values will be developed further in future research. In addition, the system of disaster weather forecasting will be enhanced further, using different spatial data mining techniques.

REFERENCES

ARNAUD Y, DESBOIS M, MAIZI J, 1992. Automatic tracking and characterization of African convective systems on meteosat pictures[J]. *Journal of Applied Meteorology*, 31: 443–453.

BREIMAN L, FRIEDMAN J H, OLSHEN R A, *et al*., 1984. *Classification and Regression Trees* [M]. Monterey, CA: Wadsworth International Group.

CARVALHO L M V, JONES C, 2001. A satellite method to identify structural properties of mesoscale convective systems based on maximum spatial correlation tracking technique (MASCOTTE)[J]. *Journal of Applied Meteorology*, 40: 1683–1701.

HOLDER L B, 1995. Intermediate decision trees[A]. In: *Proc. 14th Intl. Joint Conf. on Artificial Intelligence* (*AAAI*'1995) [C]. Montreal: Morgan Kaufmann, 1056–1062.

JIANG Ji-xi, FAN Mei-zhu, 2002. Convective clouds and mesoscale systems over the Tibetan Plateau in summer [J]. *Journal of Atmospheric Sciences*, 26(2): 263–270. (in Chinese)

KITAMOTO A, 2002. Spatial-temporal data mining for typhoon image collection[J]. *Journal of Intelligence Information Systems*, 19(1): 25-41.

KOPERSKI K, HAN J, 1995. Discovery of spatial association rules in geographic information databases[A]. In: *Proc. 4th Intl. Symposium on large Spatial Databases* (*SSD*'95)[C]. Maine: Springer, 47–66.

LEE R S T, LIU J N K, 1999. An automatic satellite interpretation of tropical cyclone patterns using elastic graph dynamic link model[J]. *IJPRAI*, 13: 1251–1270.

LEE R S T, LIU J N K, 2000. ATMOSPHERE: "Automatic track mining and objective satellite pattern hunting system using enhanced RBF and EGDLM [A]. In *Proceedings of* 17th *National Conference on Artificial Intelligence* (*AAAI*'2000) [C]. Austin: AAAI Press, 603–608.

MACHADO L A T, ROSSOW W B, GUEDES R L *et al*., 1998. Life cycle variations of mesoscale convective systems over the America [J]. *Mon. Wea. Rev*., 126: 1630–1654.

MADDOX R A, 1980. Mesoscale convective complexes [J]. *Bull. Amer. Meteor. Soc*., 61: 1374–1387.

SALVATORE Ruggieri, 2002. Efficient C4.5 [J]. *IEEE Transactions on Knowledge and Data Engineering*, 14(2): 438–444.

SHAN Yin, LIN Hui, FU Wei-ci, et al., 2003. The features of MCS during its initiation over Tibetan Plateau in summer [J]. *Journal of Tropical Meteorology*, 19: 61–66. (in Chinese)

WEISS S M, KAPOULEAS I, 1989. An empirical comparison of pattern recognition, neural nets, and machine learning classification methods[A]. In: *Proc. 11th Intl. Joint Conf. on Artificial Intelligence (IJCAI'89)* [C]. Detroit: Morgan Kaufmann, 781–787.

ZHOU Zhi-hua, CHEN Shi-fu, CHEN Zhao-qiao, 1999. Mining typhoon knowledge with neural networks[A]. In: *Proc. 11th IEEE Int. Conf. on Tools with Artificial Intelligence (ICTAI'99)* [C]. Los Alamitos: IEEE Computer Society, 325–326.